

Piecewise Deterministic Markov Processes for Bayesian Neural Networks

Ethan Goan¹Dimitri Perrin¹Kerrie Mengersen¹Clinton Fookes¹¹Queensland University of Technology

Abstract

Inference on modern Bayesian Neural Networks (BNNs) often relies on a variational inference treatment, imposing violated assumptions of independence and the form of the posterior. Traditional MCMC approaches avoid these assumptions at the cost of increased computation due to its incompatibility to subsampling of the likelihood. New Piecewise Deterministic Markov Process (PDMP) samplers permit subsampling, though introduce a model-specific inhomogeneous Poisson Process (IPPs) which is difficult to sample from. This work introduces a new generic and adaptive thinning scheme for approximate sampling from these IPPs, and demonstrates how this approach can accelerate the application of PDMPs for inference in BNNs. Experimentation illustrates how inference with these methods is computationally feasible, can improve predictive accuracy, MCMC mixing performance, and provide informative uncertainty measurements when compared against other approximate inference schemes.

1 INTRODUCTION

Since Hamiltonian Monte Carlo (HMC) was first developed for Bayesian inference Neal [2012], sampling methods have seen relatively little application to Bayesian Neural Networks (BNNs). Flexibility, inference diagnostics and asymptotic guarantees of HMC comes at the cost of computational complexity as each data point needs to be used to compute the entire likelihood, and to perform Metropolis Hastings corrections. As models and data sets have grown, this expense has not been offset by the considerable performance increase in computational hardware. A recent study found that the fitting of a HMC model for ResNet20 required a computational cost equivalent to 60 million SGD epochs to

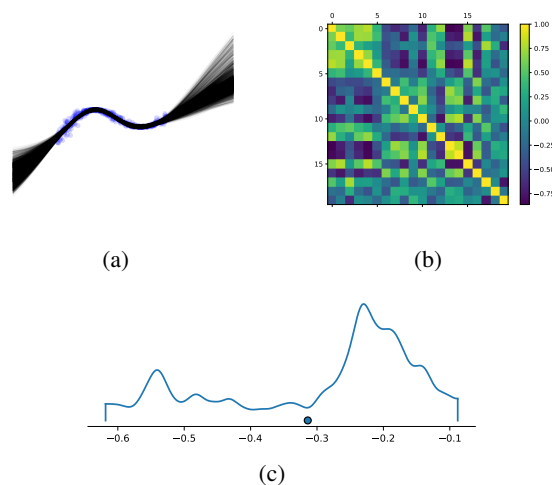


Figure 1: Example of correlations between the parameters in the first layer of a BNN for a simple regression task. Plot (a) samples of predictive posterior from proposed method, (b) correlation between all parameters on the first layer, (c) kernel density estimate for a single parameter.

obtain only 240 samples from three chains Izmailov et al. [2021].

To circumnavigate the computational expense, much research has explored the application of approximate inference through the lens of Variational Inference (VI) Jordan et al. [1999], Wainwright and Jordan [2008], Blei et al. [2017] or through exploiting properties of SGD Mandt et al. [2017]. VI replaces the true target distribution with an approximate distribution that can be easily manipulated, typically using a mean-field approach where independence between parameters is assumed. These methods are attractive due to their reduced computational complexity and their amenability to stochastic optimisation. However, the suitability of these methods relies heavily on the expressiveness of the approximate posterior to accurately model the true distribution. Given the known correlations and frequent multi-

modal structure amongst parameters within BNNs Barber and Bishop [1998], MacKay [1995], a mean-field approximation can be unsuitable for accurate inference. Figure 1 illustrates these properties for a simple BNN. Stochastic gradient MCMC methods such as Stochastic Gradient Langevin Dynamics (SGLD) aim to address this issue but requires prohibitively small and decreasing learning rates to target the posterior that limits their applicability Nagapetyan et al. [2017].

This work explores a new set of “exact” inference methods based on Piecewise Deterministic Markov Processes (PDMPs) Davis [1984] to perform Bayesian inference. PDMP methods can maintain the true posterior as its invariant distribution during inference whilst permitting subsampling of the likelihood at each update. This property is attractive for BNNs which typically are of large dimension in terms of parameters and data sets. Furthermore, previous research has highlighted PDMP methods for favourable performance in terms of mixing and sampling efficiency Bouchard-Côté et al. [2018], Bierkens et al. [2019], Wu and Robert [2017], Bierkens et al. [2020]. The dynamics of these samplers are simple to simulate, though simulating the times to update these dynamics is controlled by an Inhomogeneous Poisson Process (IPP) which can be difficult to sample. This work explores an adaptive procedure to approximate sampling of these event times to allow for approximate inference within the context of BNNs. The contributions of this paper are the following,

- Propose a novel adaptive thinning method for approximate sampling from IPPs events
- Develop a GPU-accelerated package for applying these methods to general models
- Evaluate the performance of these methods applied to computer vision tasks using BNNs;
- Evaluate the suitability of PDMP samplers for BNNs and investigate how they can improve predictive accuracy, calibration and posterior exploration when compared against SGLD.

MCMC methods have often been seen as computationally prohibitive for models with many parameters or where modern large data sets are used. It is hoped that this work will demonstrate that approximate inference using MCMC approaches for BNNs can be practically feasible, offer insightful results, and to show how we can leverage exact methods for approximate inference to more accurately target posterior distributions in BNNs.

2 PRELIMINARIES

Following the description from Fearnhead et al. [2018], PDMP are defined by three key components: piecewise deterministic dynamics, an event rate, and the transition

kernel. For inference, the goal is to design these three key components such that we can use the properties of a PDMP to sample from the posterior distributions of our parameters ω . We represent the deterministic dynamics as $\Psi(\omega, \mathbf{v}, t)$, where \mathbf{v} is an auxiliary velocity variable to guide posterior exploration with known distribution $\Phi(\mathbf{v})$ and t represents time. At random events, these dynamics are updated in accordance to a specified transition kernel. Upon an update event, the piecewise deterministic dynamics of the system update according to the kernel, and the state ω at the time of the update event serves as the starting position for the next segment such that they are all connected.

An IPP with rate function $\lambda(\omega(t), \mathbf{v}(t))$ governs the update times for the dynamics. All rate functions in this work rely upon the negative joint log probability of the model,

$$U(\omega) = -\log(p(\omega)p(\mathcal{D}|\omega)), \quad (1)$$

where $p(\omega)$ is a prior or reference measure and $p(\mathcal{D}|\omega)$ is our likelihood. If these three components are suitably defined, these processes can sample from a given posterior distribution. For derivations on how to design these components to target a posterior distribution, the reader can refer to Fearnhead et al. [2018], Vanetti et al. [2017], Davis [1993]. We now introduce the samplers used within this work.

2.1 BOUNCY PARTICLE SAMPLER

The dynamics of the Bouncy Particle Sampler (BPS) Bouchard-Côté et al. [2018] are given by $\Psi(\omega, \mathbf{v}, t) = \omega^i + \mathbf{v}^i t$, where the superscripts indicate a deterministic segment. The velocity remains constant within these segments and the parameter space is explored linearly. The velocity is updated at event times given by $\tau \sim \text{IPP}(\lambda(\omega(t)), \mathbf{v})$, where,

$$\lambda(\omega(t), \mathbf{v}) = \max\{0, \nabla U(\omega) \cdot \mathbf{v}^i\}. \quad (2)$$

Once an event time is sampled, the state of our variable “bounces” according to a lossless inelastic Newtonian collision,

$$\mathbf{v}^{i+1} = \mathbf{v}^i - 2 \frac{\nabla U(\omega^{i+1}) \cdot \mathbf{v}^i}{\|\nabla U(\omega^{i+1})\|^2} \nabla U(\omega^{i+1}) \quad (3)$$

where ω^{i+1} represents the end of the previous segment at time τ , and serves as the starting position for the following segment. The BPS provides linear dynamics that are simple to simulate, though relies only on local gradient information, which can lead to inefficient exploration for BNNs. Preconditioning can allow us to address this.

2.2 PRECONDITIONED BPS

To accelerate posterior exploration in directions of interest, we can precondition the gradients to include more infor-

mation about the structure of our posterior space. Introduction of a preconditioning matrix A results in new dynamics of $\Psi(\omega, \mathbf{v}, t) = \omega^i + A\mathbf{v}^i t$, and a new event rate, $\lambda(\omega(t), \mathbf{v}) = \max\{0, \mathbf{v} \cdot A\nabla U(\omega + \mathbf{v}t)\}$. Upon events, the velocity is updated according to,

$$\mathbf{v}^{i+1} = \mathbf{v}^i - 2 \frac{A\nabla U(\omega^{i+1}) \cdot \mathbf{v}^i}{\|A\nabla U(\omega^{i+1})\|^2} A\nabla U(\omega^{i+1}). \quad (4)$$

With careful choice of A , exploration along certain axis can be appropriately scaled. Pakman et al. [2017] propose a preconditioner similar to Li et al. [2015], though our preliminary experimentation found inconsistent results when applied to BNNs. Instead, we opt to build on the approach of Bertazzi and Bierkens [2020], where we use variance information of our samples to precondition our dynamics. We choose the preconditioner such that $A = \text{diag}(\Sigma^{\frac{1}{2}})$, where Σ is the estimated covariance in our sample found during a warm-up period. As such, we refer to this sampler as the σ BPS.

2.3 BOOMERANG SAMPLER

The Boomerang Sampler Bierkens et al. [2020] introduces non-linear dynamics for both parameter and velocity terms, and the inclusion of a Gaussian reference measure for the parameters and velocity $\mathcal{N}(\omega_*, \Sigma_*) \otimes \mathcal{N}(0, \Sigma_*)$. The first term in this reference measure will appear in the target distribution similar to a prior in the joint probability over parameters, and the second as the known distribution for the velocity component. The parameters ω_* and Σ_* can be specified as traditional prior, or can be specified in an empirical approach where they are learnt from the data. Within this work, we will set ω_* to the MAP estimate. In the original paper, Σ_* is set to the inverse of the Hessian, however, this can be computationally prohibitive for BNNs. Instead, we approximate the diagonal of the Hessian matrix as,

$$\Sigma_* = \gamma \left[\sum_{i=0}^N \frac{\partial}{\partial \omega^2} - \log p(\mathbf{y}_i | \mathbf{x}_i, \omega) \right]^{-1} \quad (5)$$

where N is the number of mini-batches present, $\mathbf{x}_i, \mathbf{y}_i$ represents data from the i 'th mini-batch, and γ is a hyperparameter to adjust the scale as needed.

Unlike the BPS samplers, the velocity does not remain constant between events. The dynamics of the Boomerang sampler for ω and \mathbf{v} within events are given by $\Psi(\omega, \mathbf{v}, t)_\omega = \omega_* + (\omega^i - \omega_*) \cos(t) + \mathbf{v}^i \sin(t)$, $\Psi(\omega, \mathbf{v}, t)_\mathbf{v} = -(\omega^i - \omega_*) \sin(t) + \mathbf{v}^i \cos(t)$, where the subscripts denote the parameter and velocity trajectory within the deterministic segment. The event rate is the same as the BPS, and the starting velocity for the next segment is updated upon events as,

$$\mathbf{v} = \mathbf{v} - 2 \frac{\nabla U(\omega) \cdot \mathbf{v}}{\left\| \Sigma_*^{\frac{1}{2}} \nabla U(\omega) \right\|^2} \Sigma_* \nabla U(\omega). \quad (6)$$

2.4 VELOCITY REFRESHMENT

All of the samplers introduced fail to target the posterior explicitly when using the above dynamics alone. Introduction of a refreshment step rectifies this, which is governed by a homogeneous PP $\tau_{ref} \sim \lambda(\lambda_{ref})$. When $\tau_{ref} < \tau$, the velocity is instead randomly sampled from the known reference distribution $\Phi(\mathbf{v})$, and τ_{ref} is used for the update event time. For BPS samplers in this work, we use a refreshment distribution of the form $\mathcal{N}(0, \sigma^2)$, where for the BPS σ is a hyper-parameter to be set and for the σ BPS is used as the standard deviation learnt during the warmup stage, and the Boomerang sampler requires $\Phi(\mathbf{v}) = \mathcal{N}(0, \Sigma_*)$. A summary of PDMP algorithms for inference is described in Algorithm 1.

Algorithm 1: Application of PDMP samplers for Inference

Result: Samples from posterior distribution

while Sampling do

```

// Simulate event time
// eventtimes in this work
// simulated with Algorithm 2
 $\tau \sim \text{PP}(\lambda(\omega, \mathbf{v}))$ ;
// Simulate time of refresh event
 $\tau_{ref} \sim \text{PP}(\lambda_{ref})$ ;
 $\tau^i = \min(\tau, \tau_{ref})$ ;
// find end of current
// piecewise-deterministic
// segment, which will form start
// of next segment
 $\omega^{i+1} = \Psi(\omega, \mathbf{v}, \tau^i)_\omega$ ;
if  $\tau^i = \tau$  then
| // update according kernel
|  $\mathbf{v}^{i+1} = R(\omega^{i+1}, \mathbf{v}^i)$ ;
else
| // refresh velocity
|  $\mathbf{v}^{i+1} \sim \Phi(\mathbf{v})$ ;
end

```

end

2.5 PROBLEMS WITH THE EVENT RATE

With the deterministic dynamics illustrated in these samplers, the main challenge in implementation of these methods is due to the sampling of the event times. Analytic sampling from IPP($\lambda(t)$) requires being able to invert the integral of the event rate w.r.t. time,

$$\Lambda(t) = \int_0^\tau \lambda(t) dt = \int_0^\tau \max\{0, \mathbf{v} \cdot A\nabla U(\omega(\mathbf{v}, t))\} dt, \quad (7)$$

where $A = \mathbf{I}$ for the BPS and Boomerang samplers. Inverting the above integral is feasible only for simple models. A

general case for sampling from IPPs is available through thinning Lewis and Shedler [1979]. This requires introducing an additional rate function that we can sample from $\mu(t)$ that is also a strict upper bound on the event rate function of interest such that $\mu(t) \geq \lambda(t)$ for all $t \geq 0$.

The efficiency of any thinning scheme relies on the tightness of the upper bound; the greater the difference between the upper bound and the true rate, the more likely a proposed time will be rejected when sampling. Pakman et al. [2017] propose a Bayesian linear regression method to generate an upper bound suitable for thinning, though requires the calculation of variance within gradients to formulate a suitable upper bound. They calculate this variance empirically, which requires computing the gradient for each data point individually within a mini-batch. This computation prohibits use for BNNs where automatic differentiation software is used. Furthermore, the selection of a suitable prior distribution for this is non-trivial for neural networks. In the next section, we address this issue by instead introducing an interpolation-based scheme for creating efficient and adaptive approximate upper bounds that avoids excessive gradient computations and the need to specify a prior on the approximate bound.

3 ADAPTIVE BOUNDS FOR SAMPLERS

3.1 SAMPLING FROM IPPS WITH LINEAR EVENT RATES

Our goal is to create a piecewise-linear envelope $h(t)$ that will serve as an approximate upper bound of our true event rate, where each segment in $h(t)$ is represented by $a_i t + b_i$. This envelope will serve as the event rate for a proposal IPP that will be suitable for use with the thinning method of Lewis and Shedler [1979]. Acceptance of an event time t is given by,

$$U \leq \frac{\lambda(t)}{h(t)}, \quad (8)$$

where $U \sim \text{Uniform}[0, 1]$. We begin by building on the work of Klein and Roberts [1984] to demonstrate how to sample times from an IPP with a piecewise-linear event rate which we can use with thinning.

Within our proposal IPP with rate $h(t)$, we wish to generate the next event time t_i given the previous event t_{i-1} . The probability of events occurring within the range of $[t_{i-1}, t_i]$ is given by Devroye [2006],

$$F(x) = 1 - \exp\{-\Lambda(t_i) - \Lambda(t_{i-1})\}. \quad (9)$$

t_i is distributed as,

$$t_{i-1} + \Lambda^{-1}(U), \quad (10)$$

where $U \sim \text{Uniform}[0, 1]$. For linear segments, the solution

to this system can be written as Klein and Roberts [1984],

$$t_i = -b_i/a_i + \sqrt{(b_i^2 + a_i^2 t_{i-1}^2 + 2a_i b_i t_{i-1} - 2a_i \log(1 - U))}/a_i. \quad (11)$$

This provides a framework for sampling from IPPs with a linear event rate. We now describe how we create a piecewise-linear envelope for a proposal process that can be used for thinning.

3.2 PIECEWISE INTERPOLATION FOR EVENT THINNING

We begin by introducing a modified event rate for which we will form our envelope,

$$\hat{\lambda}(\omega(t), \mathbf{v}) = \max\{0, \alpha \nabla U(\omega) \cdot \mathbf{v}^i\}, \quad (12)$$

where $\alpha \geq 1$ is a positive scaling factor to control the tightness of the approximate bound on the rate. The use of $\hat{\lambda}$ for creating our envelope is valid, since for values of $\alpha \geq 1$, $\hat{\lambda}(t) \geq \lambda(t)$. The scaling factor included in this event rate is designed to provide flexibility to end users with respect to computational time and bias that will be introduced during inference. The closer α is to one, the lower the probability for rejection of proposed event times, but the greater the probability that the generated event rate will not be a strict upper bound.

Our goal is to create a piecewise-linear upper bound suitable for proposing event times using Equation 11. To achieve this we have two growing sets, one for proposed event times $T = \{t_0, \dots, t_n\}$ and the value of the adjusted event rates at these times $L = \{\hat{\lambda}(t_0), \dots, \hat{\lambda}(t_n)\}$ for which we can create a set of functions,

$$h(t) = a_i t + b_i, \quad t \geq t_i. \quad (13)$$

The values for a_i and b_i are found by interpolating between the points $(t_{i-1}, \hat{\lambda}(t_{i-1}))$ and $(t_i, \hat{\lambda}(t_i))$.

At the beginning of every deterministic PDMP segment, the sets T and L will be empty. To initialise the sets and create our first linear segment, we evaluate the event rate at two points, $t_0 = 0$ and $t = t_{init}$, where $t_{init} > t_0$. To evaluate the values for a_0 and b_0 , we interpolate between these two segments. Once the values for the first linear segment are found, t_0 and $\hat{\lambda}(t_0)$ are appended to their corresponding sets, and t_{init} and $\hat{\lambda}(t_{init})$ are discarded. With this initial linear segment, we can propose a time t_i through Equation 11. This proposed time is either accepted or rejected from Equation 8.

If the proposed time is accepted, then the dynamics of the PDMP sampler are updated at the given event time and the sets T and L are cleared, ready to be re-initialised for

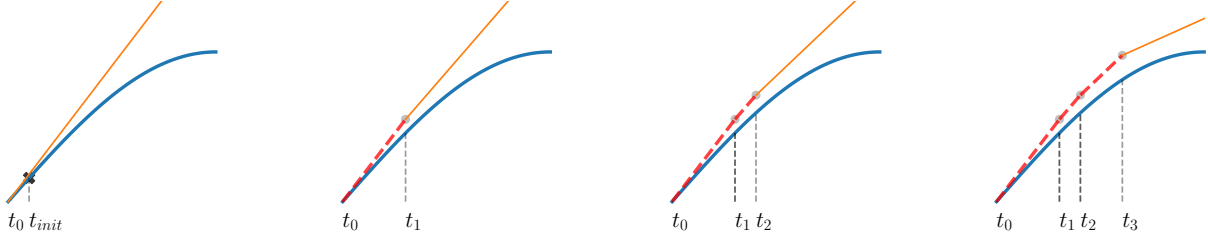


Figure 2: Example of the progression of the proposed envelope scheme used for thinning. The blue line represents the true event rate, orange section depicts the active regions for which we sample a new proposal time, and the red section depicts previous segments in the envelope. Starting from the left, an initial segment is found through interpolation between time points t_0 and t_{init} . In the next segment, active regions of the envelope are found by interpolating between the two prior points, which extends to create a new segment to propose times. This process continues until a proposed time is accepted from thinning.

the new dynamics. If the time is rejected, the proposed time t_i and envelope evaluation $\lambda(t_i)$ are appended to their respective sets, and a new linear segment is calculated to interpolate between this rejected proposal and the previous elements in the sets T and L . The rejected proposal time will serve as the new starting point (t_{i-1}) for the new linear segment to propose the next time using Equation 11. This will continue until the proposed event time is accepted. This process depicted visually in Figure 2 and summarised in Algorithm 2.

Within this work, we limit ourselves to models where the envelope provided by $h(t)$ will only be an approximate upper bound, meaning bias will likely be introduced during inference. Diagnosis and correction of this can be identified through the acceptance ratio $\lambda(t)/h(t)$; if this value is greater than one, the condition of $h(t)$ being a local upper bound is violated. The amount of potential bias introduced can be mitigated by increasing the scaling factor α in Equation 12 at the expense of increasing computation load. We also introduce an additional rejection condition such that if $\lambda(t)/h(t) > R$, then we will reject the proposed time. For this work, $R = 2$. These properties are investigated in Supp. Material A. In the following sections, we evaluate the proposed event thinning scheme for BNNs to identify the suitability of different samplers for inference in these challenging models, and how they can outperform other stochastic approximation methods in terms of calibration, posterior exploration, sampling efficiency and predictive performance.

4 RELATED WORK

The samplers used within this work require the use of an additional reference process to provide velocity refreshments. The Generalised BPS Wu and Robert [2017] is an updated variant of the BPS algorithm that incorporates a stochas-

Algorithm 2: Sampling event rate using proposed adaptive thinning method.

Result: Proposed PDMP Event Time τ

Initialize T, L ;

Evaluate $(0, \lambda(0)), (t_{init}, \lambda(t_{init}))$;

$i = 1$;

Compute a_i, b_i ;

$T_0 \leftarrow 0, L_0 \leftarrow \lambda(t)$;

Discard $t_{init}, \lambda(t_{init})$;

while not accepted do

// propose event time with t_{i-1}, a_i
and b_i

$t_i \sim PP(h(t))$;

$u \sim \text{Uniform}[0, 1]$;

$r = \lambda(t_i)/h(t)$;

// if valid proposal

if $u \leq r$ and $r < R$ then

// sample is accepted

$\tau = t_i$;

accepted = True;

end

else

// increment counter

$i += 1$;

$T_i \leftarrow t_i, L_i \leftarrow \lambda(t_i)$;

// update linear segment

$a_i, b_i = \text{update}(L, T)$;

end

end

tic update of the velocity which alleviates the need for a refreshment process. Simulations have shown comparable performance to the BPS for simple models and how it can reduce the need for fine-tuning the reference parameter τ_{ref} .

Another prominent sampler is the Zig-Zag Process (ZZP) [Bierkens et al., 2019], where at events the dynamics of a single parameter are updated. For the one-dimensional case, this sampler represents the same process as the BPS. This sampler has shown favourable results in terms of mixing performance and can achieve ergodicity for certain models where the BPS cannot. A key characteristic of this method is that each parameter is assigned an individual event rate, making implementation for high-dimensional BNN models challenging.

Another class of algorithms designed for subsampling are discrete stochastic MCMC methods Wenzel et al. [2020], Chen et al. [2014], Ma et al. [2015], Welling and Teh [2011], Li et al. [2015]. These models have shown favourable performance, with a recent variant achieving comparable predictive accuracy on the ImageNet data set Heek and Kalchbrenner [2019]. Compared to algorithms related to PDMPs, it has been shown that high variance related to naive subsampling limits these methods to provide only an approximation to the posterior Betancourt [2015]. The bias that is introduced due to subsampling can be controlled by reducing the step-size for these methods at the expense of mixing performance and posterior exploration Nagapetyan et al. [2017], Brosse et al. [2018], Teh et al. [2016]. We investigate the effect of this property for SGLD and compare performance with PDMP samplers in the following section.

5 EXPERIMENTS

We now validate the performance of PDMPs using the proposed event sampling method on a number of synthetic and real-world data sets for regression and classification. To analyse performance for predictive tasks, the predictive posterior needs to be evaluated. In this work, we discretise samples from the trajectory to allow for Monte Carlo integration,

$$p(y^*|x^*, \mathcal{D}) = \int \pi(\omega)p(y^*|\omega, x^*)d\omega \\ \approx \frac{1}{N} \sum_{i=1}^N p(y^*|\omega_i, x^*) \quad \omega_i \sim \pi(\omega), \quad (14)$$

where parameter samples of $\omega^{(i)}$ are taken from the values encountered at event times. Experimentation is first conducted on synthetic data sets to allow us to easily visualise predictive performance and uncertainty in our models, followed by more difficult classification tasks with Bayesian Convolutional Neural Networks (CNNs) on real data sets. For all experimentation, we set our scaling factor from Equation 12 to $\alpha = 1.0$ to promote computational efficiency. To enable these experiments, we deliver a Python package titled Tensorflow PDMP (TPDMP). This package utilises the Tensorflow Probability library Dillon et al. [2017], allowing for hardware acceleration and graph construction of all our models to accelerate computation. We deliver kernels to

implement the BPS, σ BPS, and Boomerang sampler with our proposed event thinning scheme. Code is available at <https://github.com/egstatsml/tpdmp.git>.

5.1 REGRESSION AND BINARY CLASSIFICATION WITH SYNTHETIC DATA

To visualise predictive performance and uncertainty estimation, regression and binary classification tasks are formed on synthetic data sets. Description of the networks used for these tasks is described in Supp. Material E. Before sampling, a MAP estimate was first found using stochastic optimisation, and was used to initialise each sampler. 2,000 samples were generated using each sampling method, with each sampler initialised from the same MAP estimate. The σ BPS requires an additional warmup period to identify suitable values for the preconditioner. We achieve this by performing 1,000 initial samples using the BPS, and standard deviation parameters used for the preconditioner are estimated from these samples using the Welford algorithm Welford [1962]. These preconditioner values are then fixed throughout the sampling process. The PDMP methods are compared against SGLD which starts with a learning rate that decays to zero as required Welling and Teh [2011], Nagapetyan et al. [2017], and with no decay of the learning rate as is commonly done in practice (SGLD-ND). Examples of the predictive posterior distribution for regression and binary classification are shown in Figures 3 and 4 respectively, with full analysis in Supp. Material B. All PDMP models are fit with the proposed adaptive event thinning procedure.

Results from these experiments affirm that inference from the PDMP models is suitable for predictive reasoning, with low variance seen within the range of observed data and greater variance as distance from observed samples increases. We similarly see an increase in uncertainty along the decision boundary, which is a desirable property. This is in contrast to SGLD, which is able to provide low variance predictions for in-distribution data, but offers less predictive uncertainty whilst extrapolating, for even in the case for larger non-decreasing learning rates. This highlights the known limitations of SGLD, that with a decaying learning rate it can fail to explore the posterior, and with a larger non-decreasing learning rate will converge to dynamics offered by traditional SGD Brosse et al. [2018], Nagapetyan et al. [2017].

These tests indicate promising performance in terms of predictive accuracy and uncertainty estimates. To further demonstrate classification performance, we move to larger and more complicated models for performing regression and classification on real-world data sets.

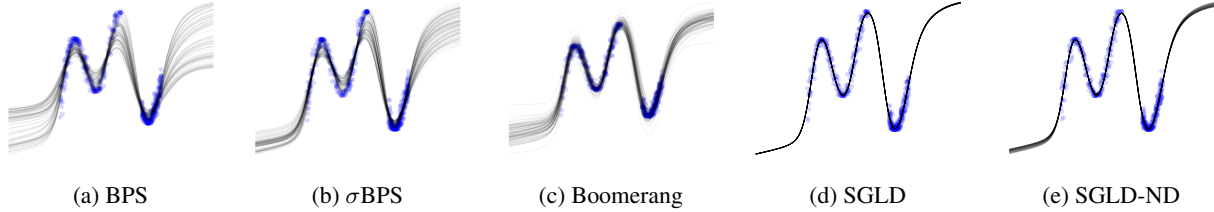


Figure 3: Examples of the different PDMP samplers using the proposed event thinning procedure on synthetic regression task compared against SGLD with decaying learning rate and constant learning rate (SGLD-ND).

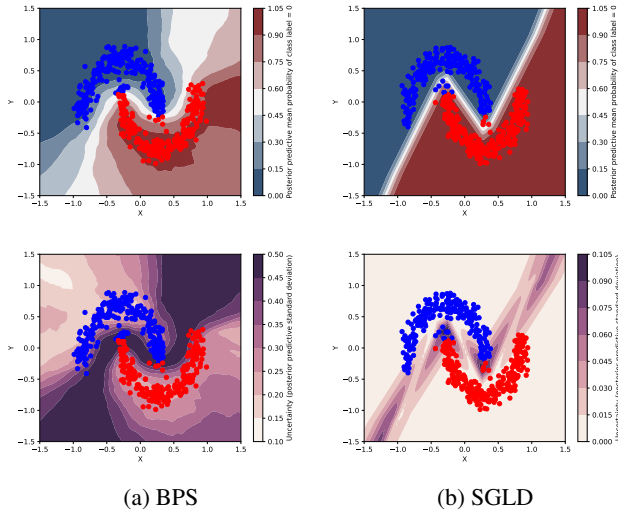


Figure 4: Examples of the predictive mean and variance for synthetic classification task. Left column illustrates results using the BPS and the right using SGLD. We see increased uncertainty for the BPS outside the range of observed data, whilst SGLD shows greater certainty.

5.1.1 UCI-Datasets

We further evaluate the performance of the PDMP samplers enabled by the proposed event sampling scheme on datasets from the UCI repository Newman et al. [1998]. In Table 1, we show performance metrics on the Boston houses dataset, with the Naval, Energy, Yacht, and Concrete datasets evaluated in Supp. Material E.2. Each model is fit with 1,000 samples. For these experiments, we further include the naive Stochastic Gradient Hamiltonian Monte Carlo (SGHMC) Chen et al. [2014]. Predictive performance of these models is measured with Root Mean Squared Error (RMSE) and Negative Log-Likelihood (NLL). Sampling efficiency is evaluated with Effective Sample Size (ESS) Robert et al. [1999]. Due to the high dimension of our models, we perform PCA on returned samples and project them onto the first principal component to report ESS on the direction of greatest variance within samples.

From these results, we see SGLD and SGHMC provide a

Table 1: Summary of predictive performance using PDMP samplers with the proposed event time sampling methods on the Boston Houses dataset. Negative log-likelihood (NLL) and Root Mean Squared Error (RMSE) are reported. Effective sample size (ESS) is measured over the first principal component of samples. Results are shown over 5 independent runs with standard deviations reported.

Inference	NLL ↓	RMSE ↓	ESS ↑
BPS	0.96 ± 0.00	2.76 ± 0.11	2.71 ± 0.02
σ BPS	0.96 ± 0.01	2.73 ± 0.12	2.70 ± 0.01
Boomerang	0.96 ± 0.01	2.77 ± 0.13	901.07 ± 105.03
SGLD	0.96 ± 0.00	2.68 ± 0.01	2.89 ± 0.00
SGHMC	0.96 ± 0.00	2.69 ± 0.05	2.71 ± 0.00

slight improvement in terms of RMSE, though we see that the Boomerang Sampler considerably outperforms both of these methods in terms of sample efficiency. This result follows from the previous sections where we see that SGLD frequently converges to the SGD solution space, whilst the PDMP samplers can explore the posterior space. Additional results in Supp. Material E.2 further validate these results, and show how predictive performance can be improved with PDMP samplers.

5.2 MULTI-CLASS CLASSIFICATION

We now evaluate the performance of the proposed sampling procedures on the popular MNIST LeCun et al. [1998], Fashion MNIST Xiao et al. [2017], SVHN Netzer et al. [2011], CIFAR-10 and CIFAR-100 Krizhevsky and Hinton [2009] data sets using CNNs. For MNIST and Fashion-MNIST, the LeNet5 architecture was used whilst for SVHN, CIFAR-10, and CIFAR-100 the modified ResNet20 architecture from Wenzel et al. [2020] was used. For the Boomerang Sampler, we follow the original Bierkens et al. [2020] and implement a flat prior, and for other samplers a normal prior is used.

Similar to the experiments on regression, a MAP estimate is found and used to initialise each sampler. 2,000 samples for each model are then generated, though a thinning factor of 10 is used to reduce the number of returned samples used for

Table 2: Summary of predictive performance using PDMP samplers with the proposed event time sampling methods. Negative log-likelihood (NLL) is reported, along with calibration measured using the expected calibration error (ECE) Guo et al. [2017]. Effective sample size (ESS) is measured over the first principal component of samples. Mean and standard deviation in results presented over 5 independent runs.

Inference	ACC \uparrow	NLL \downarrow	ECE \downarrow	ESS \uparrow
MNIST				
BPS	0.99 \pm 0.00	0.08 \pm 0.04	5.22 \pm 3.44	2.88 \pm 0.07
σ BPS	0.99 \pm 0.00	0.02 \pm 0.00	0.48 \pm 0.22	2.72 \pm 0.02
Boomerang	0.99 \pm 0.00	0.03 \pm 0.00	0.85 \pm 0.37	175.26 \pm 29.38
SGLD	0.99 \pm 0.00	0.02 \pm 0.00	0.19 \pm 0.02	22.74 \pm 0.18
SGLD-ND	0.99 \pm 0.00	0.02 \pm 0.00	0.15 \pm 0.01	3.00 \pm 0.00
SGHMC	0.99 \pm 0.00	0.02 \pm 0.00	0.17 \pm 0.02	2.71 \pm 0.00
Fashion-MNIST				
BPS	0.91 \pm 0.00	0.25 \pm 0.00	1.00 \pm 0.38	2.73 \pm 0.04
σ BPS	0.91 \pm 0.00	0.30 \pm 0.01	3.94 \pm 0.30	2.74 \pm 0.02
Boomerang	0.91 \pm 0.00	0.28 \pm 0.01	3.82 \pm 2.24	143.05 \pm 31.32
SGLD	0.90 \pm 0.01	0.30 \pm 0.01	3.09 \pm 1.49	102.52 \pm 84.14
SGLD-ND	0.91 \pm 0.00	0.33 \pm 0.00	4.71 \pm 0.01	2.97 \pm 0.00
SGHMC	0.91 \pm 0.00	0.34 \pm 0.01	4.88 \pm 0.13	2.71 \pm 0.00
SVHN				
BPS	0.95 \pm 0.00	0.18 \pm 0.00	0.61 \pm 0.09	2.71 \pm 0.02
σ BPS	0.95 \pm 0.00	0.19 \pm 0.01	0.63 \pm 0.18	2.75 \pm 0.02
Boomerang	0.95 \pm 0.00	0.21 \pm 0.01	3.58 \pm 0.82	172.02 \pm 40.73
SGLD	0.96 \pm 0.00	0.16 \pm 0.00	1.33 \pm 0.03	21.84 \pm 0.25
SGLD-ND	0.96 \pm 0.00	0.16 \pm 0.00	1.34 \pm 0.00	2.97 \pm 0.00
SGHMC	0.95 \pm 0.00	0.19 \pm 0.00	0.83 \pm 0.27	2.71 \pm 0.00
CIFAR-10				
BPS	0.80 \pm 0.00	0.67 \pm 0.00	4.91 \pm 0.65	2.70 \pm 0.02
σ BPS	0.79 \pm 0.01	0.72 \pm 0.01	8.55 \pm 0.64	2.73 \pm 0.02
Boomerang	0.81 \pm 0.00	0.59 \pm 0.02	4.17 \pm 1.55	200.00 \pm 0.00
SGLD	0.81 \pm 0.00	1.01 \pm 0.00	15.32 \pm 0.04	54.96 \pm 18.20
SGLD-ND	0.81 \pm 0.00	0.99 \pm 0.00	15.15 \pm 0.01	2.85 \pm 0.00
SGHMC	0.80 \pm 0.00	0.96 \pm 0.00	14.64 \pm 0.15	2.71 \pm 0.00
CIFAR-100				
BPS	0.63 \pm 0.00	1.43 \pm 0.01	10.16 \pm 0.21	2.72 \pm 0.02
σ BPS	0.63 \pm 0.00	1.42 \pm 0.00	8.70 \pm 0.00	2.80 \pm 0.00
Boomerang	0.63 \pm 0.01	1.42 \pm 0.08	12.67 \pm 3.26	54.96 \pm 18.20
SGLD	0.64 \pm 0.00	1.42 \pm 0.00	11.24 \pm 0.32	26.79 \pm 0.73
SGLD-ND	0.64 \pm 0.00	1.45 \pm 0.00	12.22 \pm 0.05	2.69 \pm 0.00
SGHMC	0.63 \pm 0.00	1.46 \pm 0.00	12.63 \pm 0.12	2.71 \pm 0.00

prediction to 200. For these models, we measure predictive performance and calibration through the Accuracy, NLL, and Expected Calibration Error (ECE) Guo et al. [2017], and similarly measure sampling efficiency using the ESS with on samples after performing PCA. A full description of the models used, and experiment parameters is shown in Supp. Material E.3. Table 2 summarises the results of these experiments.

These results highlight favourable performance for PDMP samplers. The BPS and σ BPS samplers frequently provide more calibrated predictions in terms of ECE, whilst maintaining comparable predictive accuracy to SGLD methods. Most importantly, we note the Boomerang sampler con-

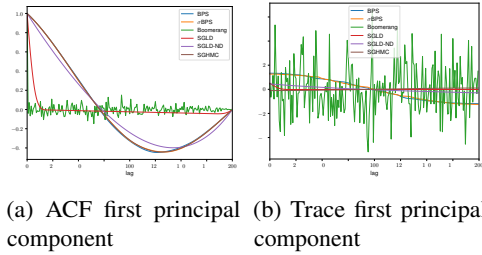


Figure 5: Example of ACF and trace plots for the first principal component of the samples from network fit on SVHN dataset.

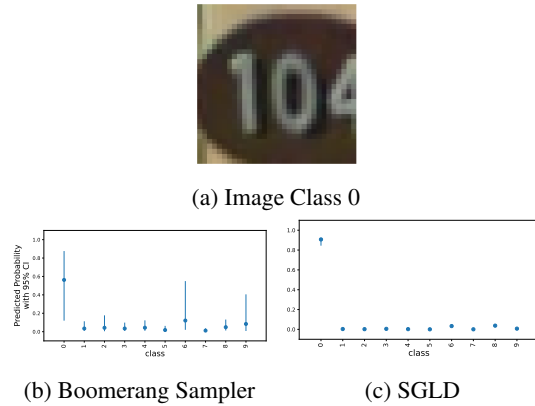


Figure 6: Examples from predictive posterior for difficult-to-classify samples from SVHN. Top row shows the original image and the bottom row shows the predictive distribution for the Boomerang sampler and SGLD. The mean for each class is represented by the dot, and the 95% credible intervals shown with the error bars.

sistently outperforms other samplers in terms of effective sample size, whilst also promoting competitive predictive accuracy and calibration. This highlights the potential for these samplers for probabilistic inference within neural networks.

With measures of predictive performance and ESS within our models, we wish to further investigate the mixing properties of the samplers presented within to identify how well the posterior space is being explored. ESS only gives a measure to approximate the number of independent samples within our MCMC chain, though we are also interested in how well the support for the posterior is being explored. Given the large number of parameters seen within a BNN, it is infeasible to evaluate the coordinate trace and auto-correlation plots for individual parameters as is typically done for MCMC models. Instead, we again perform PCA to reduce the dimension of our data and investigate the trace plots of the first principal component as illustrated in Figure. 5. From these figures, we can identify strong correlation between samples from the BPS, σ BPS, SGHMC, and SGLD-ND solutions. SGLD offers reduced correlation

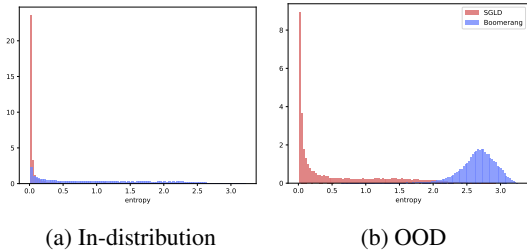


Figure 7: Entropy histograms comparing SGLD and Boomerang sampler fit on the CIFAR-10 dataset. OOD data represented by SVHN. We see the predictive entropy from the Boomerang sampler increases as desired for OOD data, whilst SGLD remains overly confident for erroneous samples.

in samples, however as seen in the trace plot, samples fail to explore the posterior and instead converge to a steady state, whilst the Boomerang sampler provides considerably reduced correlation and more favourable mixing, however we note in Supp. Material C that the Boomerang sampler can exhibit a mode seeking behaviour due to the nature of the reference measure. Convergence of the SGLD samples can be attributed to the reduction in learning rate required to target the posterior. We verify this result in Supp. Material C, where we provide further analysis into results from all networks and remaining principal components. The effect of this convergence in terms of predictive uncertainty is illustrated within Figure 6, where the PDMP sampler is able to provide more meaningful uncertainty estimates for difficult-to-classify samples, and the SGLD predictive results converge to that similar of a point estimate. Additional examples of the predictive distributions is shown in Supp. Material H.

Probabilistic methods have shown favourable performance in terms of Out of Distribution (OOD) detection Grathwohl et al. [2019], Maddox et al. [2019]. Given the point-estimate-like nature of the results returned by SGLD, we wish to compare with results from the Boomerang sampler to see if both can offer similar performance for OOD data. We see in Figure 7 that the Boomerang sampler offers greater entropy for OOD data, indicating a desirable increase in aleatoric uncertainty. Additional analysis is provided in Supp. Material G.

6 DISCUSSION AND LIMITATIONS

Whilst the PDMP methods have shown favourable performance in terms of predictive accuracy, calibration and uncertainty in BNNs, there are certain challenges with fitting them. The PDMP samplers used within this work are designed to target the joint distribution,

$$p(\omega, \mathbf{v}) = \pi(\omega)\Phi(\mathbf{v}) \quad (15)$$

where $\pi(\omega)$ is the target posterior and $\Phi(\mathbf{v})$ is the distribution of the auxiliary velocity components which must be set by users in the form of the refreshment distribution. For the BPS and σ BPS samplers, it has been shown that with a reference distribution may be a Gaussian or restricted to the unit hypersphere Bouchard-Côté et al. [2018], DURMUS et al. [2020]. For the Boomerang sampler, the velocity distribution is designed with respect to a reference measure to ensure invariance to the target distribution, such that $\Phi(\mathbf{v}) = \mathcal{N}(0, \Sigma_*)$, where Σ_* is the same factor used to precondition the dynamics. The choice in distribution used for the velocity component has an explicit effect on the mixing capabilities of the models when applied to BNNs. We demonstrate this effect in Supp. Material D.1. We find that a velocity distribution with too much variance can cause effects similar to that of divergences seen in HMC and NUTS. Furthermore, we see that with variance set too low, the samplers can fail to explore the posterior sufficiently to provide the desired meaningful uncertainty estimates. A similar effect can be seen for the choice of refreshment rate, which we investigate in Supp. Material D.2. We highlight these limitations as areas for future research to enable robust application of PDMP methods for BNNs.

The Boomerang sampler as implemented within this work and the original paper is probabilistic, though is not purely Bayesian. This is due to the reference measure being identified through the data itself. A strictly Bayesian approach can be recovered by setting the reference measure and associated preconditioner matrix from a prior distribution, though we would lose some favourable sampling performance offered by this sampler. We can view the approach implemented within similar to an empirical Bayes, where we are gleaning information about the reference measure for the Boomerang sampler from the data itself. Given the difficulty of specifying a meaningful and informative prior, and the success seen when using empirical priors for BNNs Krishnan et al. [2020], we believe the use of such an approach for the Boomerang sampler is justified.

7 CONCLUSION

Within this work, we demonstrate how PDMPs can be used for BNNs. We provide a flexible piecewise linear bound to enable sampling of event times within these frameworks that permits inference in BNNs. A GPU-accelerated software package is offered to increase the availability of PDMPs for a wide array of models. Experimentation on BNNs for regression and classification indicates comparable or improved predictive performance and calibration, though were able to consistently improve sampling efficiency and uncertainty estimation when compared against existing stochastic inference methods.

8 CORRIGENDUM

The published version of this paper contained a missing term in Equation 11 that has been corrected. Furthermore an error in the software for this paper was identified where the scaling term to correct for mini-batch sizes for the unbiased gradient estimates was not being called. Experiments have been rerun with software corrected and additional information provided in the supplementary material highlighting how samplers can be used to explore the posterior space for BNNs.

References

- David Barber and Christopher M Bishop. Ensemble learning in bayesian neural networks. *Nato ASI Series F Computer and Systems Sciences*, 168:215–238, 1998.
- Andrea Bertazzi and Joris Bierkens. Adaptive schemes for piecewise deterministic monte carlo algorithms. *arXiv preprint arXiv:2012.13924*, 2020.
- Michael Betancourt. The fundamental incompatibility of scalable hamiltonian monte carlo and naive data subsampling. In *International Conference on Machine Learning, ICML’15*, pages 533–540. JMLR.org, 2015.
- Joris Bierkens, Paul Fearnhead, Gareth Roberts, et al. The zig-zag process and super-efficient sampling for bayesian analysis of big data. *The Annals of Statistics*, 47(3):1288–1320, 2019.
- Joris Bierkens, Sebastiano Grazi, Kengo Kamatani, and Gareth Roberts. The boomerang sampler. *arXiv preprint arXiv:2006.13777*, 2020.
- David M Blei, Alp Kucukelbir, and Jon D McAuliffe. Variational inference: A review for statisticians. *Journal of the American statistical Association*, 112(518):859–877, 2017.
- Alexandre Bouchard-Côté, Sebastian J Vollmer, and Arnaud Doucet. The bouncy particle sampler: A nonreversible rejection-free markov chain monte carlo method. *Journal of the American Statistical Association*, 113(522):855–867, 2018.
- Nicolas Brosse, Alain Durmus, and Eric Moulines. The promises and pitfalls of stochastic gradient langevin dynamics. In *Advances in Neural Information Processing Systems*, pages 8268–8278, 2018.
- Tianqi Chen, Emily Fox, and Carlos Guestrin. Stochastic gradient hamiltonian monte carlo. In *International conference on machine learning*, pages 1683–1691, 2014.
- Mark HA Davis. Piecewise-deterministic markov processes: a general class of non-diffusion stochastic models. *Journal of the Royal Statistical Society: Series B (Methodological)*, 46(3):353–376, 1984.
- Mark HA Davis. *Markov models & optimization*, volume 49. CRC Press, 1993.
- Luc Devroye. Nonuniform random variate generation. *Handbooks in operations research and management science*, 13:83–121, 2006.
- Joshua V Dillon, Ian Langmore, Dustin Tran, Eugene Brevdo, Srinivas Vasudevan, Dave Moore, Brian Patton, Alex Alemi, Matt Hoffman, and Rif A Saurous. Tensorflow distributions. *arXiv preprint arXiv:1711.10604*, abs/1711.10604, 2017.
- ALAIN DURMUS, ARNAUD GUILLIN, and PIERRE MONMARCHÉ. Geometric ergodicity of the bouncy particle sampler. *The Annals of Applied Probability*, 30(5):2069–2098, 2020.
- Paul Fearnhead, Joris Bierkens, Murray Pollock, Gareth O Roberts, et al. Piecewise deterministic markov processes for continuous-time monte carlo. *Statistical Science*, 33(3):386–412, 2018.
- Will Grathwohl, Kuan-Chieh Wang, Joern-Henrik Jacobsen, David Duvenaud, Mohammad Norouzi, and Kevin Swersky. Your classifier is secretly an energy based model and you should treat it like one. In *International Conference on Learning Representations*, 2019.
- Chuan Guo, Geoff Pleiss, Yu Sun, and Kilian Q Weinberger. On calibration of modern neural networks. In *International conference on machine learning*, pages 1321–1330. PMLR, 2017.
- Jonathan Heek and Nal Kalchbrenner. Bayesian inference for large scale image classification. *arXiv preprint arXiv:1908.03491*, 2019.
- Pavel Izmailov, Sharad Vikram, Matthew D Hoffman, and Andrew Gordon Wilson. What are bayesian neural network posteriors really like? *arXiv preprint arXiv:2104.14421*, 2021.
- Michael I Jordan, Zoubin Ghahramani, Tommi S Jaakkola, and Lawrence K Saul. An introduction to variational methods for graphical models. *Machine learning*, 37(2):183–233, 1999.
- Robert W. Klein and Stephen D. Roberts. A time-varying poisson arrival process generator. *Simulation*, 43:193–195, 1984.
- Ranganath Krishnan, Mahesh Subedar, and Omesh Tickoo. Specifying weight priors in bayesian deep neural networks with empirical bayes. In *Proceedings of the AAAI Conference on Artificial Intelligence*, volume 34, pages 4477–4484, 2020. URL <https://ojs.aaai.org/index.php/AAAI/article/view/5875>.

- Alex Krizhevsky and Geoffrey Hinton. Learning multiple layers of features from tiny images. 2009.
- Yann LeCun, Léon Bottou, Yoshua Bengio, and Patrick Haffner. Gradient-based learning applied to document recognition. *Proceedings of the IEEE*, 86(11):2278–2324, 1998.
- PA W Lewis and Gerald S Shedler. Simulation of nonhomogeneous poisson processes by thinning. *Naval research logistics quarterly*, 26(3):403–413, 1979.
- Chunyuan Li, Changyou Chen, David Carlson, and Lawrence Carin. Preconditioned stochastic gradient langevin dynamics for deep neural networks. *arXiv preprint arXiv:1512.07666*, 2015.
- Yi-An Ma, Tianqi Chen, and Emily Fox. A complete recipe for stochastic gradient mcmc. In C. Cortes, N. D. Lawrence, D. D. Lee, M. Sugiyama, and R. Garnett, editors, *Advances in Neural Information Processing Systems 28*, pages 2917–2925. Curran Associates, Inc., 2015. URL <http://papers.nips.cc/paper/5891-a-complete-recipe-for-stochastic-gradient-mcmc.pdf>.
- David JC MacKay. Probable networks and plausible predictions—a review of practical bayesian methods for supervised neural networks. *Network: computation in neural systems*, 6(3):469–505, 1995.
- Wesley J. Maddox, Pavel Izmailov, Timur Garipov, Dmitry P. Vetrov, and Andrew Gordon Wilson. A simple baseline for bayesian uncertainty in deep learning. In Hanna M. Wallach, Hugo Larochelle, Alina Beygelzimer, Florence d’Alché-Buc, Emily B. Fox, and Roman Garnett, editors, *Advances in Neural Information Processing Systems 32: Annual Conference on Neural Information Processing Systems 2019, NeurIPS 2019, December 8-14, 2019, Vancouver, BC, Canada*, pages 13132–13143, 2019. URL <https://proceedings.neurips.cc/paper/2019/hash/118921efba23fc329e6560b27861f0c2-Abstract.html>.
- Stephan Mandt, Matthew D Hoffman, and David M Blei. Stochastic gradient descent as approximate bayesian inference. *Journal of Machine Learning Research*, 18:1–35, 2017.
- Tigran Nagapetyan, Andrew B Duncan, Leonard Hasenclever, Sebastian J Vollmer, Lukasz Szpruch, and Konstantinos Zygalakis. The true cost of stochastic gradient langevin dynamics. *arXiv preprint arXiv:1706.02692*, 2017.
- Radford M Neal. *Bayesian learning for neural networks*, volume 118. Springer Science & Business Media, 2012.
- Yuval Netzer, Tao Wang, Adam Coates, Alessandro Bis-sacco, Bo Wu, and Andrew Y Ng. Reading digits in natural images with unsupervised feature learning. In *NIPS workshop on deep learning and unsupervised feature learning*, volume 2011, page 5, 2011.
- D.J. Newman, S. Hettich, C.L. Blake, and C.J. Merz. Uci repository of machine learning databases, 1998. URL <http://www.ics.uci.edu/~mllearn/MLRepository.html>.
- Ari Pakman, Dar Gilboa, David Carlson, and Liam Paninski. Stochastic bouncy particle sampler. In *International Conference on Machine Learning*, pages 2741–2750, 2017.
- Christian P Robert, George Casella, and George Casella. *Monte Carlo statistical methods*, volume 2. Springer, 1999.
- Yee Whye Teh, Alexandre H Thiery, and Sebastian J Vollmer. Consistency and fluctuations for stochastic gradient langevin dynamics. *Journal of Machine Learning Research*, 17, 2016.
- Paul Vanetti, Alexandre Bouchard-Côté, George Deligiannidis, and Arnaud Doucet. Piecewise-deterministic markov chain monte carlo. *arXiv preprint arXiv:1707.05296*, 2017.
- Martin J Wainwright and Michael Irwin Jordan. *Graphical models, exponential families, and variational inference*, volume 1. Now Publishers Inc, 2008.
- BP Welford. Note on a method for calculating corrected sums of squares and products. *Technometrics*, 4(3):419–420, 1962.
- Max Welling and Yee W Teh. Bayesian learning via stochastic gradient langevin dynamics. In *Proceedings of the 28th international conference on machine learning (ICML-11)*, pages 681–688, 2011.
- Florian Wenzel, Kevin Roth, Bastiaan S. Veeling, Jakob Swiatkowski, Linh Tran, Stephan Mandt, Jasper Snoek, Tim Salimans, Rodolphe Jenatton, and Sebastian Nowozin. How good is the bayes posterior in deep neural networks really? In *International Conference of Machine Learning*, 2020.
- Changye Wu and Christian P Robert. Generalized bouncy particle sampler. *arXiv preprint arXiv:1706.04781*, art. arXiv:1706.04781, Jun 2017.
- Han Xiao, Kashif Rasul, and Roland Vollgraf. Fashion-mnist: a novel image dataset for benchmarking machine learning algorithms. *arXiv preprint arXiv:1708.07747*, 2017.

Piecewise Deterministic Markov Processes for Bayesian Neural Networks (Supplementary Material)

Ethan Goan¹

Dimitri Perrin¹

Kerrie Mengersen¹

Clinton Fookes¹

¹Queensland University of Technology

A TIGHTNESS OF PROPOSED APPROXIMATE UPPER BOUND

The key contribution within this work is the proposal of a new generic and data-dependent thinning method to approximately sample event times from within PDMP samplers. The quality of this thinning method relies on two key components; the tightness of the envelope and its ability to provide a strict upper bound. We want the envelope used to be able to be as close to the true event rate as possible without reducing below it. This enables maximum efficiency of thinning methods by reducing the likelihood of a proposed event time will be rejected.

Previous works have relied on performing experimentation on simple well-defined models where derivation of a strict and exact upper bound???? Derivation for a strict upper bound is infeasible for neural networks, though we can assess the quality of our event thinning method by analysing the acceptance ratio in Equation 8 from the body of the paper. We want this ratio to be as close to one as possible without exceeding it, otherwise, the envelope section used to propose the time is below the true event rate. We assess the distribution of these acceptance ratios for varying values of α from Equation 12 in the body of the paper in Figure 1 and we illustrate the result on predictive performance and computational load in Table 1.

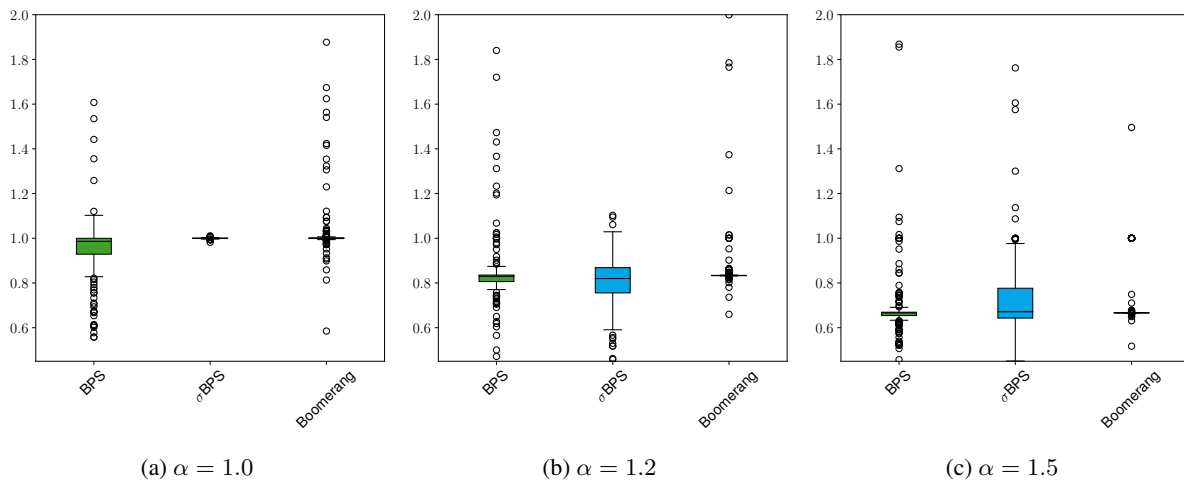


Figure 1: Distribution of acceptance ratios for event thinning across the different PDMP samplers used within this work for varying levels of α . All models are fit on the MNIST data set as described in Section 5.2.

From this experiment, we note that for $\alpha = 1$ we see tight clustering of acceptance ratios around one for the σ BPS and Boomerang Sampler. Whilst this may initially indicate a tight bound being found, it will in fact indicate that our approximate upper bound was initially violated and then corrected. This occurs if our rate for the event switching $\lambda(t)$ is zero and then rapidly increases. If our event rate changes such that the acceptance ratio $\lambda(t)/h(t)$ is greater than our rejection condition

Table 1: Summary of predictive performance with and timings as the scaling value of α is increased for the PDMP samplers demonstrated within. All models are fit to the MNIST dataset using the Lenet5 architecture.

α	Inference	ACC	NLL	ECC	Time
$\alpha = 1.0$	BPS	0.9896	0.0536	2.66	71
	σ BPS	0.9923	0.0227	0.4127	121
	Boomerang	0.9919	0.0230	0.139	78
$\alpha = 1.2$	BPS	0.9902	0.0638	3.74	74
	σ BPS	0.9922	0.0247	2.7380	118
	Boomerang	0.9861	0.0456	33.2281	135
$\alpha = 1.5$	BPS	0.987	0.0614	2.909	79
	σ BPS	0.9925	0.0244	0.3858	126
	Boomerang	0.9922	0.0232	0.1651	160

factor R , the proposal will be rejected with hopes to correct it on subsequent samples. Whilst the proposed method is capable of correcting the event rate on the next proposal, bias will be introduced during inference due to the initial proposal exceeding $h(t)$. We see that as α increases, the distribution of acceptance ratio for the σ BPS broadens, and from Table 1, the run-time decreases as fewer rejections due to this process occurs, whilst as α increases further, the run-time begins to increase. We can see that with $\alpha = 1.0$, we see frequent occurrences of the proposed envelope being below that of the true event rate, though as we increase the value of α , the likelihood of the approximate envelope being a strict upper bound increases. In practice, setting this scaling parameter can be achieved through the use of a small warm-up phase at the start of sampling to find a ratio that satisfies a users willingness to mitigate bias that may be induced due to the violation of the upper bound assumption. To mitigate potential bias, the value of α may be increased at the expense of a small increase in the computational demands of the thinning method as seen in Table 1. The violation of the bounds within the Boomerang sampler can be attributed to the non-linear dynamics of the process. We highlight this phenomenon as an direction for future research.

B ADDITIONAL REGRESSION AND BINARY CLASSIFICATION EXAMPLES

To further validate the predictive performance of PDMP samplers using the proposed event thinning method, we provide additional examples on easy to visualise regression tasks in Figure 2 and Figure 3 which are compared with Stochastic Gradient Langevin Dynamics (SGLD) with a decreasing learning rate as required, and a constant learning rate with no decay as is typically done in practice (SGLD-ND). For regression models, a learning rate of 10^{-5} is used, and for binary classification models the learning rate is set to 10^{-2} . The learning rate for SGLD experiments decays to zero linearly.

From these results, we further validate the predictive performance of these samplers and their ability to yield informative uncertainty information for out-of-distribution data when compared to SGLD with a decaying learning rate and a constant learning rate. We find that even with a larger value learning rate used for SGLD-ND that the sampler is unable to explore the posterior sufficiently to provide meaningful uncertainty estimates. This phenomenon has been reported in ?, where they identify that even with a larger and constant learning rate, SGLD dynamics converge to that of regular SGD.

C MIXING PERFORMANCE

In Section 5.2, experiments to investigate the mixing capabilities of the PDMP samplers were conducted using PCA to reduce the dimensionality of the samples generated from the different samplers for a single network. We extend this analysis here for all models in Figures 4, 5 and 6 for the first, second, and last principal components respectively. From these figures we can verify that the Boomerang sampler provided the greatest overall mixing across the different models and datasets, whilst SGLD consistently converges to a single solution. We further investigate this here by comparing raw parameter traces within different parts of the networks used for the MNIST and SVHN datasets. These results are shown in Figure 7, and confirms the pathology of SGLD quickly converging to a single steady-state solution, whilst the PDMP samplers are able to able to explore the posterior at all stages in the networks. We also note that the parameter traces for the Boomerang sampler a potential mode-seeking behaviour, and that the trace plots for the BPS and σ BPS explore a greater span of the posterior space. This can be attributed to the use of the reference measure within the Boomerang sampler. Whilst it was able

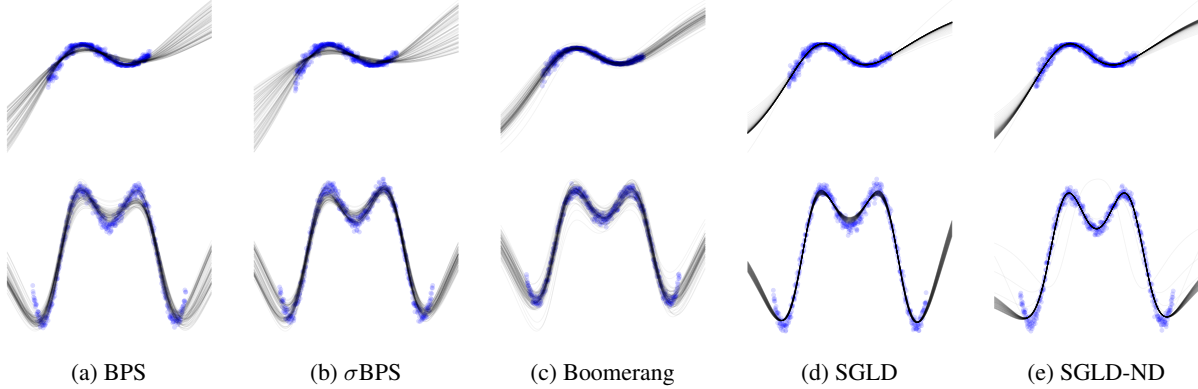


Figure 2: Example of predictive posteriors for BNN regression models across synthetic data sets. Training samples are shown in blue dots, and draws from the predictive distribution shown with black lines.

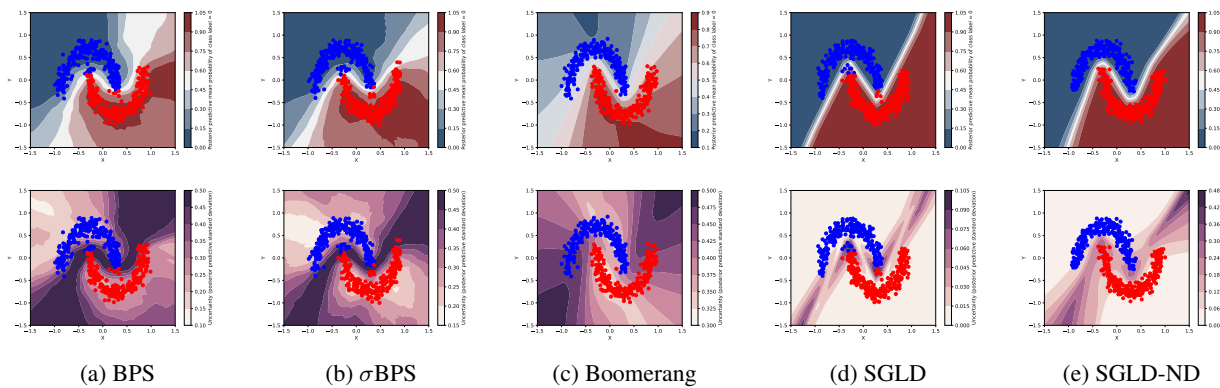


Figure 3: Examples of predictive distributions for synthetic binary classification task. Top row indicates predictive mean and bottom row illustrates variance in predictions. Best viewed on a computer screen in colour.

to consistently generate more independent samples in terms of ESS, the BPS methods may be able to traverse a greater span of the posterior space. We highlight this as an direction for future research. From this, we can verify that SGLD is converging to a steady-state solution, whilst the Boomerang sampler consistently explores the posterior space and provide improved mixing. Given the requirement for SGLD to maintain a small learning rate that approaches 0 to target the posterior π^* , these results are expected. The theoretic ability of SGLD to maintain the posterior as its invariant distribution comes at the expense mixing efficiency.

D SENSITIVITY TO HYPER-PARAMETERS

D.1 SENSITIVITY TO VELOCITY DISTRIBUTION

As noted in Section 6, we discuss the sensitivity of these PDMP Samplers for BNNs with respect to the distribution assigned to the auxiliary velocity variable. Given that the aim of this velocity variable is to guide the dynamics of the system to efficiently explore the parameter space, it needs to be set appropriately. We demonstrate this here through experimentation to highlight how poorly specified velocity distribution can corrupt inference.

Figure 8 illustrates the predictive distribution for poorly specified velocity distributions for the Boomerang sampler, though similar effects are seen amongst the other PDMP samplers when the variance for the velocity distribution is incorrectly specified. We see that the scale of the velocity component proportionately controls the mixing capabilities of the model. When variance is too low, the sampler is unable to explore beyond the MAP solution, and when too large the predictive performance can suffer. With better approximations to the diagonal of Hessian of the negative log-likelihood, the effects of this may be mitigated for the Boomerang Sampler. We highlight these behaviours of PDMP samplers applied to BNNs to

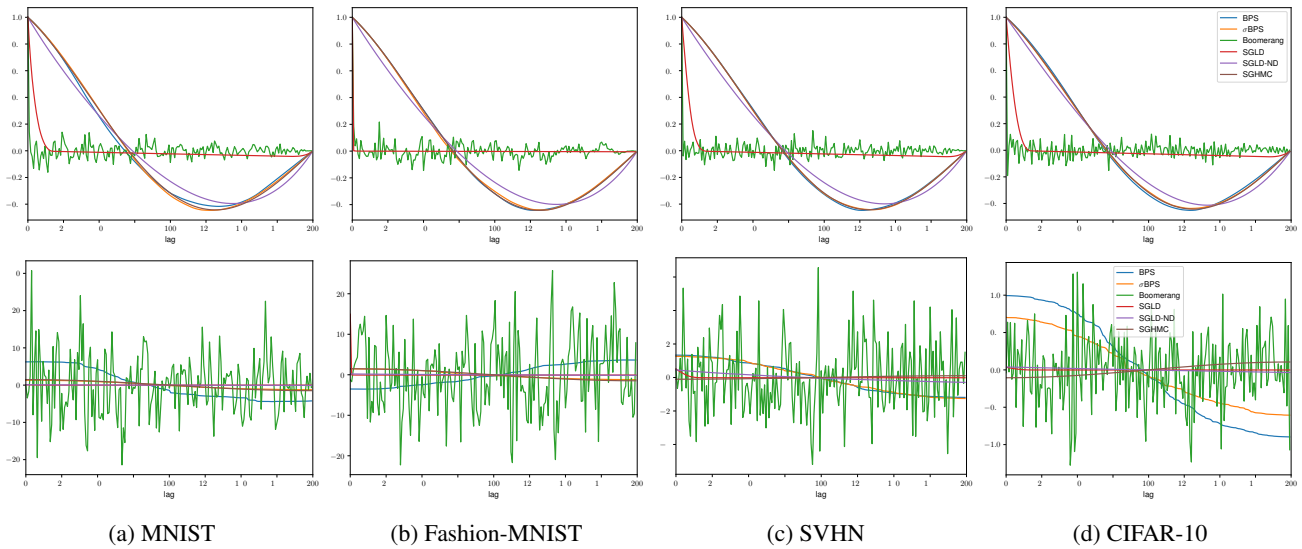


Figure 4: Plots summarising samples from tested samples projected onto first principal component. Top row represents the ACF plot, and the bottom shows the coordinate trace plot for the first principal component. Best viewed on a computer screen.

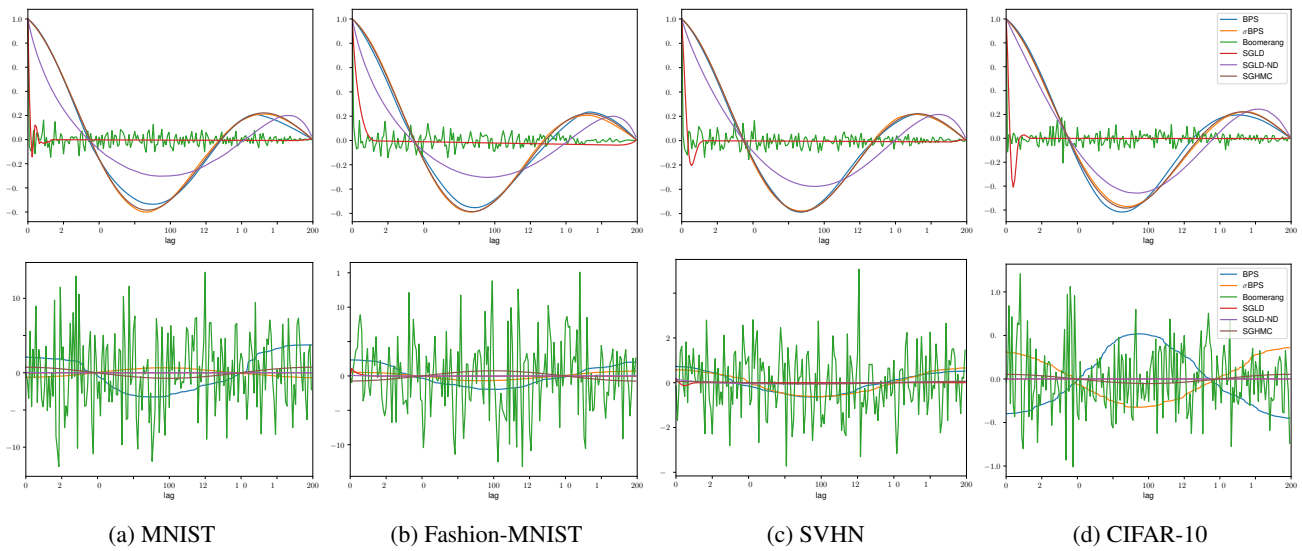


Figure 5: Plots summarising samples from tested samples projected onto second principal component. Top row represents the ACF plot, and the bottom shows the coordinate trace plot for the first principal component. Best viewed on a computer screen.

show the limitations and to provide insight into the importance of setting these parameters correctly, and areas of future research.

D.2 SENSITIVITY TO REFRESH EVENT RATE

MCMC samplers such as HMC ? and NUTS ? have step size parameters that can be adjusted and tuned for individual models. With a small step size, exploration of the posterior can be limited, and if too large then divergences in the posterior trajectory can be encountered and corrupting inference ?. The step size parameter is typically tuned during a warm-up phase before sampling is commenced to find an optimal value to maximise exploration and minimise the risk of encountering these divergences.

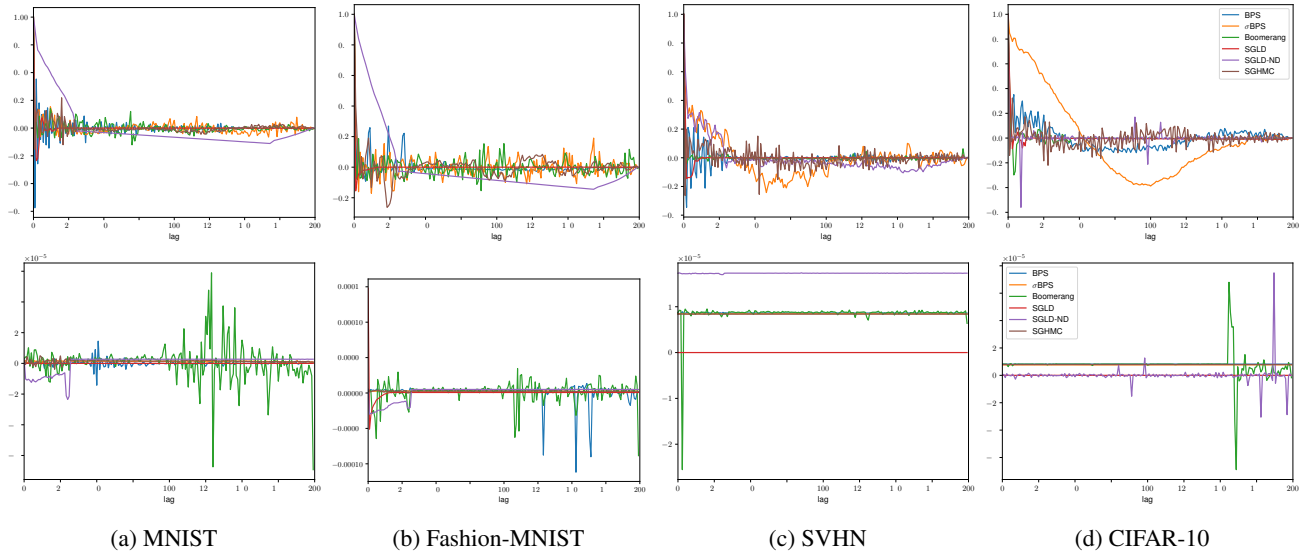


Figure 6: Plots summarising samples from tested samples projected onto last principal component. Top row represents the ACF plot, and the bottom shows the coordinate trace plot for the last principal component. Best viewed on a computer screen.

The PDMP samplers within here do not have an equivalent parameter that can be tuned to guide simulation. The trajectory of these samplers is defined solely on the transition kernel to update velocity parameters and the event rate that determines when these events occur. We can however yield a similar effect to adjusting the step size of a traditional MCMC model through our choice of event rate for our refreshment process $PP(\lambda_{ref})$.

Recall from Section 2.4 that the final event time is given by,

$$\tau_{event} = \min(\tau, \tau_{ref}) \quad (1)$$

Where $\tau \sim PP(\lambda(\omega(t), \mathbf{v}(t)))$, and $\tau_{ref} \sim PP(\lambda_{ref})$. Setting the value for τ_{ref} can implicitly control the level of exploration within our samplers. For large λ_{ref} , we will encounter smaller proposed refresh times and thus will refresh more frequently. Similarly, for larger λ_{ref} , our sampled refresh times will be larger, and τ_{event} will equal τ more frequently, and further exploration of the posterior space with these dynamics will be possible. We illustrate this in Figure 9, where we show the effects for large and smaller values of λ_{ref} .

We can see that the refresh rate can have a considerable impact on the inference quality of our model. With λ_{ref} too large, our exploration is limited and we perform excessive refreshments instead of accepting those provided by the PDMP kernel. When is too small, we can accept larger event times as specified by the PDMP sampler and can diverge away from meaningful inferences.

E SUMMARY OF MODELS USED

E.1 REGRESSION AND BINARY CLASSIFICATION MODELS FOR SYNTHETIC DATA

Regression models used within this work consist of fully-connected networks with two hidden layers, each with 25 and 10 units respectively. Tanh non-linear activations are applied after each hidden layer, and a Normal likelihood with a variance of $\sigma^2 = 0.01$ is used. MAP estimates for these networks are found with 10,000 iterations using the Adam optimiser [?](#), with each sampler initialised from the same MAP estimate.

For binary classification models, the networks consist of a fully-connected network with three hidden layers, each with 100 units. ReLU non-linear activations are applied within the network, and a Bernoulli likelihood is used. Similar to the regression tasks, MAP estimate is found with Adam.

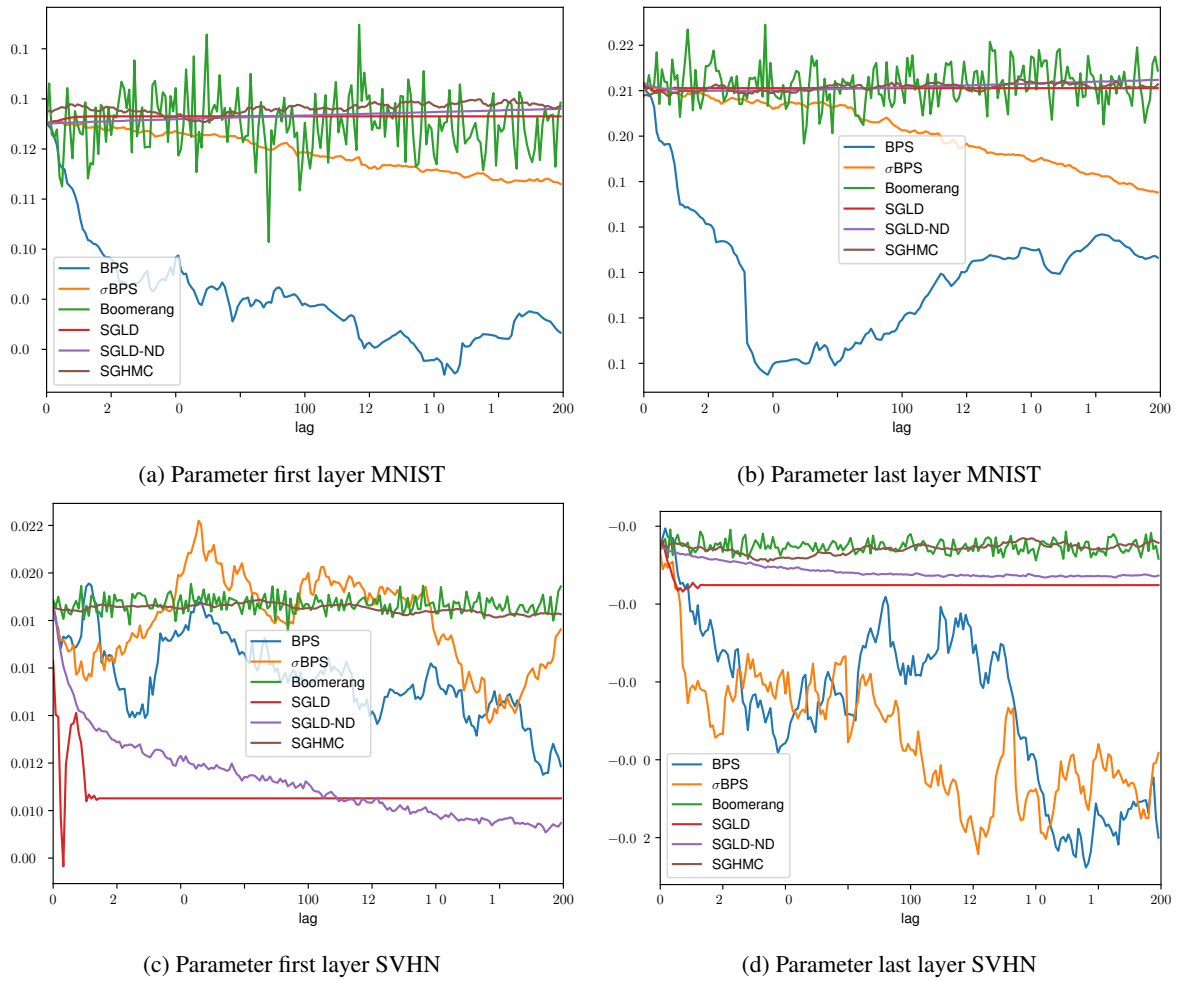


Figure 7: Trace plots comparing mixing of SGLD and the Boomerang sampler for individual weight parameters within different networks at different locations.

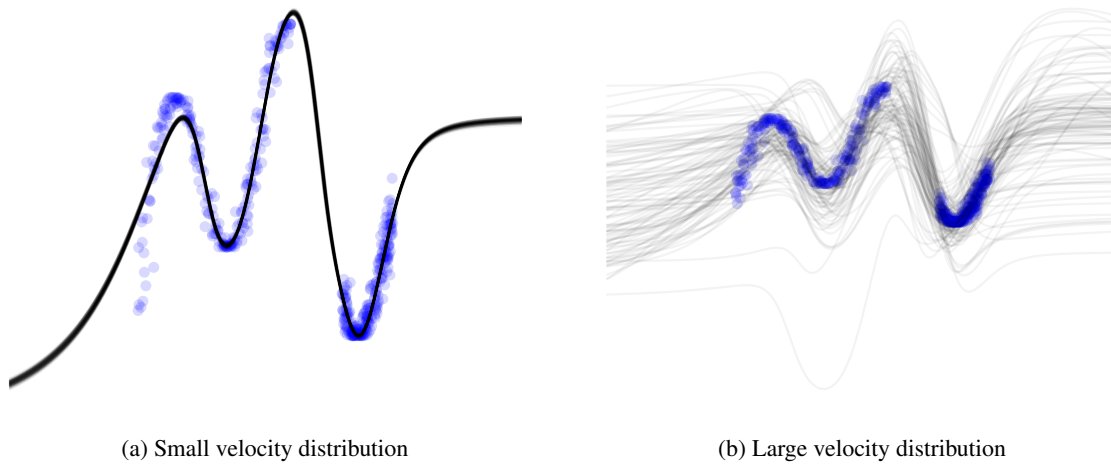


Figure 8: Effect of scale in velocity reference measure for PDMP samplers applied to BNNs.

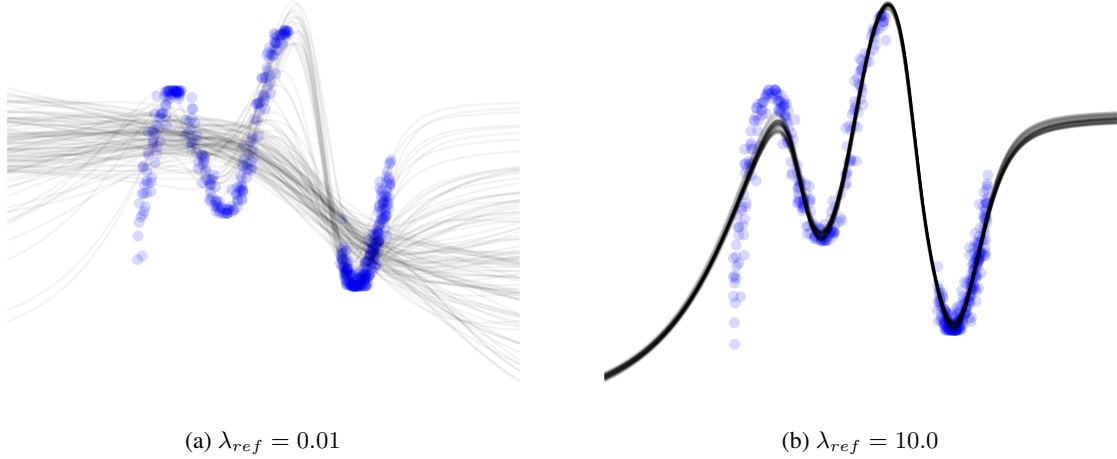


Figure 9: Effect of λ_{ref} on PDMP models applied to BNNs. Shown here is the predictive distribution found with the BPS using the proposed event rate thinning method.

E.2 ADDITIONAL UCI-DATASET RESULTS

We provide here additional results on datasets from the UCI repository?. For each dataset, a simple MLP network with a three hidden layers with 512, 256, and 128 hidden units is used, along with a ReLU activation. MAP estimates are found similar to E.1, followed by 1,000 samples generated by each method. Each experiment is run 5 times with mean results and standard deviations reported. We further include ESS as measured on from the smallest principle component of samples. Results from these experiments reflect that seen in Section 5.1.1; where the PDMP methods show comparable or improved predictive performance. The Boomerang sampler is able to consistently outperform other sampling methods in terms of ESS, with other samplers only able to match sample efficiency for the smallest principal components where exploration is smallest.

Table 2: Results on UCI-Naval Dataset

Inference	NLL	RMSE	ESS-First	ESS-Second	ESS-Last
BPS	0.96 ± 0.00	2.76 ± 0.11	2.71 ± 0.02	4.09 ± 0.05	412.68 ± 536.28
σ BPS	0.96 ± 0.01	2.73 ± 0.12	2.70 ± 0.01	4.14 ± 0.08	1000.00 ± 0.00
Boomerang	0.96 ± 0.01	2.77 ± 0.13	901.07 ± 105.03	937.24 ± 72.62	871.02 ± 288.40
SGLD	0.96 ± 0.00	2.68 ± 0.01	2.89 ± 0.00	4.45 ± 0.05	1000.00 ± 0.00
SGHMC	0.96 ± 0.00	2.69 ± 0.05	2.71 ± 0.00	4.10 ± 0.00	1000.00 ± 0.00

Table 3: Results on UCI Energy Dataset

Inference	NLL	RMSE	ESS-First	ESS-Second	ESS-Last
BPS	0.95 ± 0.00	0.00 ± 0.00	2.71 ± 0.02	4.13 ± 0.07	392.42 ± 529.69
σ BPS	0.95 ± 0.00	0.00 ± 0.00	2.73 ± 0.03	4.15 ± 0.06	800.66 ± 445.74
Boomerang	0.97 ± 0.02	0.00 ± 0.00	837.54 ± 181.39	824.77 ± 139.27	790.48 ± 276.02
SGLD	1.60 ± 0.19	0.01 ± 0.00	2.96 ± 0.01	5.74 ± 0.14	1000.00 ± 0.00
SGHMC	0.92 ± 0.00	0.00 ± 0.00	2.71 ± 0.00	4.10 ± 0.00	195.98 ± 106.67

Table 4: Results on UCI Yacht Dataset

Inference	NLL	RMSE	ESS-First	ESS-Second	ESS-Last
BPS	0.92 ± 0.00	0.97 ± 0.31	2.75 ± 0.05	4.11 ± 0.11	15.27 ± 10.84
σ BPS	0.92 ± 0.00	0.75 ± 0.01	2.72 ± 0.03	4.24 ± 0.24	1000.00 ± 0.00
Boomerang	0.92 ± 0.00	1.00 ± 0.33	732.04 ± 276.22	754.01 ± 156.27	777.24 ± 142.72
SGLD	0.92 ± 0.00	0.85 ± 0.10	3.07 ± 0.00	4.96 ± 0.05	1000.00 ± 0.00
SGHMC	0.92 ± 0.00	1.01 ± 0.13	2.71 ± 0.00	4.10 ± 0.00	224.12 ± 62.13

Table 5: Results on UCI Concrete Dataset

Inference	NLL	RMSE	ESS-First	ESS-Second	ESS-Last
BPS	0.93 ± 0.00	1.85 ± 0.03	2.72 ± 0.03	4.10 ± 0.06	592.92 ± 531.11
σ BPS	0.93 ± 0.00	1.84 ± 0.03	2.72 ± 0.01	4.15 ± 0.07	1000.00 ± 0.00
Boomerang	0.93 ± 0.00	1.92 ± 0.05	888.04 ± 250.34	821.95 ± 336.23	757.61 ± 235.83
SGLD	0.93 ± 0.00	1.87 ± 0.00	3.01 ± 0.00	4.97 ± 0.02	1000.00 ± 0.00
SGHMC	0.93 ± 0.00	1.97 ± 0.28	2.71 ± 0.00	4.10 ± 0.00	245.39 ± 49.05

E.3 CONVOLUTIONAL MODELS

For the σ BPS, an initial warm-up stage is again required, which is identical to that in Section 5.1. For MNIST and Fashion-MNIST, a batch size of 1024 is used, whilst a batch size of 512 is used for the remaining models. MAP estimates for MNIST and Fashion-MNIST datasets were found with the Adam optimiser for 10,000 iterations. SVHN and CIFAR-10 used SGD with momentum of 0.1 and 0.9 respectively for 25,000 iterations, where for CIFAR-100, required 128,000 iterations and a momentum of 0.2.

With the potential sensitivities to both refreshment rates and choice of velocity distribution $\Phi(\mathbf{v})$ identified in D, we deem it important to report the values used for fitting each model. We report these values in Table 6 alongside full predictive performance measurements and sample efficiency metrics. Within Table 6, we represent the choice of velocity distribution with the γ parameter. For Bouncy Particle Sampler (BPS), γ describes the standard deviation of the velocity distribution chosen such that,

$$\Phi(\mathbf{v}) = \mathcal{N}(0, \gamma^2). \quad (2)$$

Similarly, an initial velocity distribution is set for the σ BPS during initial warmup phase, afterwards the velocity distribution is set to $\mathcal{N}(0, \sigma^2)$. For the Boomerang sampler, γ represents the scaling factor as found in Equation 6 from the body of the paper.

F HOW WELL ARE WE REALLY EXPLORING THE POSTERIOR?

In Radford Neals influential thesis, he states that ‘‘Bayesian neural network users may have difficulty claiming with a straight face that their models and priors are selected because they are just what is needed to capture their prior beliefs about the problem’’¹. In a similar vein, we would state that any Bayesian neural network user would have a difficult time honestly saying their inference strategy has sufficiently explored the posterior, including the work proposed here. Previous research has investigated gold-standard MCMC methods for larger networks, though were unable to obtain a sufficient number of samples to maintain confidence in the levels of exploration. Although the metrics in the previous section may show sufficient results for a machine learning application, from a statistical perspective we need to further investigate the quality of our inference to justify whether we have satisfied our goal of sampling from the posterior distribution.

Previous papers for PDMP methods for MCMC have shown favourable performance in terms of mixing and sampling efficiency and has similarly outperformed methods such as SGLD. Most studies have been restricted to well-defined models; where prior information can be suitably provided and sufficient prior studies with gold standard methods such as

¹Although much important work has been conducted to establish suitable priors and model design, this statement largely remains true today.

Table 6: Summary of hyperparameters used for samplers within this work.

Dataset	Inference	λ_{ref}	γ	Time
MNIST	SGD	-	-	74
	SGLD	-	-	87
	SGLD-ND	-	-	87
	BPS	1.0	0.001	145
	σ BPS	1.0	0.0005	197
	Boomerang	1.0	0.1	151
Fashion-MNIST	SGD	-	-	74
	SGLD	-	-	87
	SGLD-ND	-	-	87
	BPS	1.0	0.001	144
	σ BPS	0.1	0.001	192
	Boomerang	1.0	0.1	156
SVHN	SGD	-	-	3465
	SGLD	-	-	3653
	SGLD-ND	-	-	3653
	BPS	0.5	0.00005	4125
	σ BPS	0.5	0.00005	4535
	Boomerang	1.0	0.1	4375
CIFAR 10	SGD	-	-	4905
	SGLD	-	-	5075
	SGLD-ND	-	-	5074
	BPS	0.5	0.00005	5614
	σ BPS	1.0	0.00005	6053
	Boomerang	0.01	0.01	5868
CIFAR 100	SGD	-	-	9811
	SGLD	-	-	9985
	SGLD-ND	-	-	9985
	BPS	0.70	0.00005	10478
	σ BPS	1.5	0.000025	10808
	Boomerang	2.0	0.01	10783

HMC and NUTS have confirmed the general geometry of the posteriors in question and the existence of a central limit theorem. Inference in BNNs is challenged by a posterior with strong multi-modality, making exploration of any sampler more difficult. This is further challenged by the comparatively large dimensional space over which we need to explore. The favourable Gaussian Process and functional properties seen by networks with infinite width ? encourage the use of large models, whilst also narrowing the typical set in which we wish to explore ?.

Another limitation is the computational complexity added with sampling-based schemes. This complexity not only includes the cost of sampling, but the increase in memory consumption. The popular ResNet-50 model contains more than 23 million parameters. To perform inference on ImageNet with a ResNet50 model using a mini-batch size of 100 samples, more than 10 thousand samples would be needed to iterate over the entire data set of over one million images. With single-point precision, these samples for a single complete iteration of the dataset would require more than 9.2GB of memory. These constraints currently limit the applicability of such methods, as evaluating predictive posteriors will require a large number of samples and many operations to read sampled values from non-volatile storage.

These limitations offer insights into areas of future research relating to sampling schemes for BNNs. The geometry of the joint posterior distribution could be improved by investigating non-local methods for preconditioning the gradients, similar to that done in Riemannian HMC ?. As seen in this work through the efficacy of the Boomerang sampler, exploitation of this geometry can considerably improve exploration of the posterior space. Finally and perhaps most importantly, bespoke design of model architecture that respects the data and includes priors that appropriately reflect domain expertise could yield posteriors that are more easily traversed and explored.

¹The commonly used variant of ImageNet is from the 2012 Large Scale Visual Recognition Challenge, which contains 1,281,167 samples ?

G IN AND OUT OF DISTRIBUTION DATA

We investigate here the performance of the different sampling methods for in and out-of-distribution (OOD) data in terms of predictive classification entropy. We have demonstrated that PDMP sampling methods present meaningful epistemic uncertainty in predictions. It is important to identify uncertainty in the final predictions that are made. Within this work, predictions are made by taking the argmax of the mean for the predictive posterior,

$$\mathbf{t} = \underset{y^* \in \mathcal{Y}}{\operatorname{argmax}} \mathbb{E}_{y^*} \left[p(y^* | x^*, \mathcal{D}) \right] \quad (3)$$

Where $p(y^* | x^*, \mathcal{D})$ is our predictive posterior. Entropy within this categorical probability vector given by this expectation can be viewed as an approximate measure for aleatoric uncertainty within our model \mathcal{M} to accompany the epistemic uncertainty given by our Bayesian models. To assess this, we compute the entropy of the expectation within Equation 3 for in-distribution data and OOD data. It is desirable to have a lower entropy for in-distribution data indicating lower predictive aleatoric uncertainty, and a larger entropy for OOD data to represent an increase in uncertainty. Figure 10 illustrates this for the models used within this work. From Figure 10, we see the SGLD provides a reduced entropy for in-distribution data, but provides

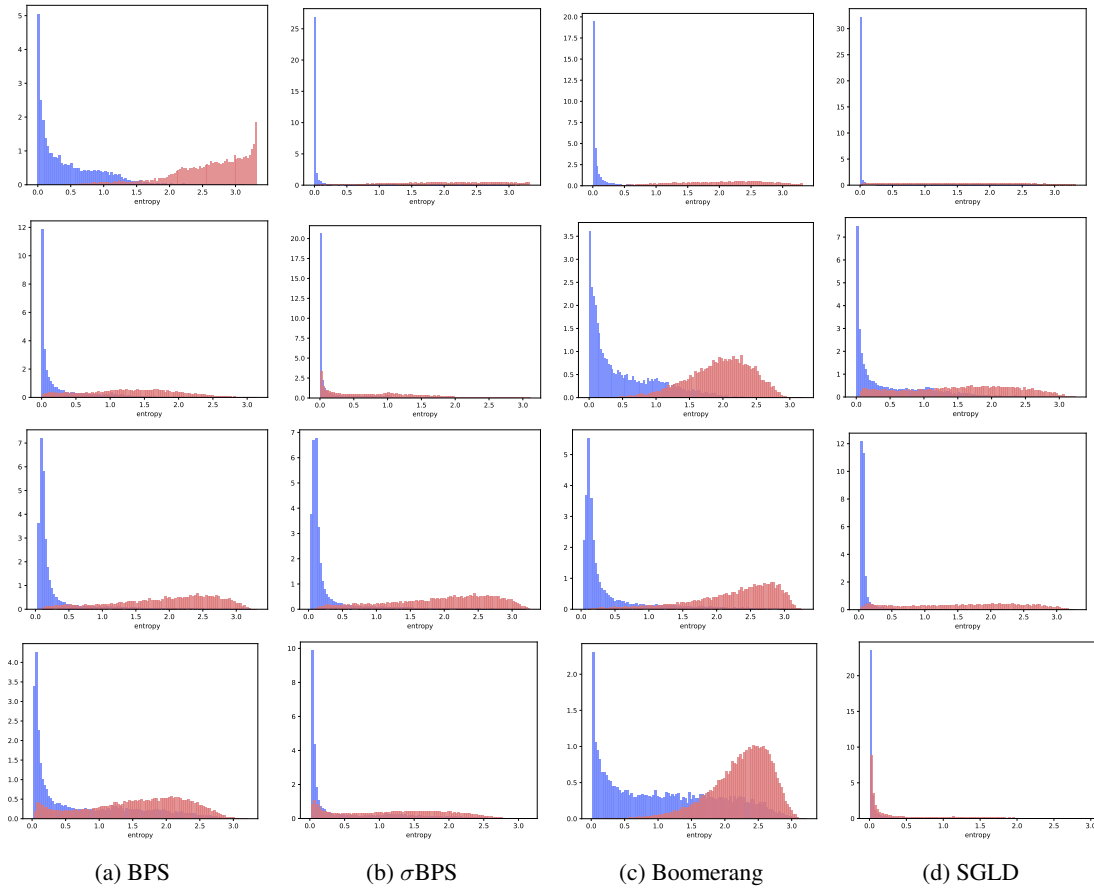


Figure 10: Entropy within the final predictive categorical vector obtained from the tested sampling methods for the different datasets used. Blue histograms indicate in-data-distribution entropy and red for OOD data. Each column represents the predictive entropy for the corresponding labelled sampler and each row for a different dataset. From top to bottom, each row is for models fit on the MNIST, Fashion MNIST, SVHN, and CIFAR-10 data respectively. MNIST and Fashion MNIST datasets are used to model in and OOD datasets for the applicable models, and similarly SVHN and CIFAR-10 to model in and OOD for respective models.

reduced levels of entropy for OOD data when compared with PDMP samplers. This highlights a favourable property for results from PDMP applications for neural networks for detection and communication of additional uncertainty for OOD data.

H EXAMPLES OF DIFFICULT TO CLASSIFY SAMPLES

Given the increasing desire to apply deep learning models in practice, the ability for them to reliably communicate uncertainty information is crucial. We expect our models to encounter difficult-to-understand scenarios. We need to be able to identify when these challenging scenarios occur and to incorporate the uncertainty encountered into final decisions. Figure 11 illustrates examples of misclassified samples from the datasets evaluated within this work, and illustrates the predictive probabilities of these models. We see that all PDMP samplers provide meaningful uncertainty information for difficult-to-classify instances within each data set.

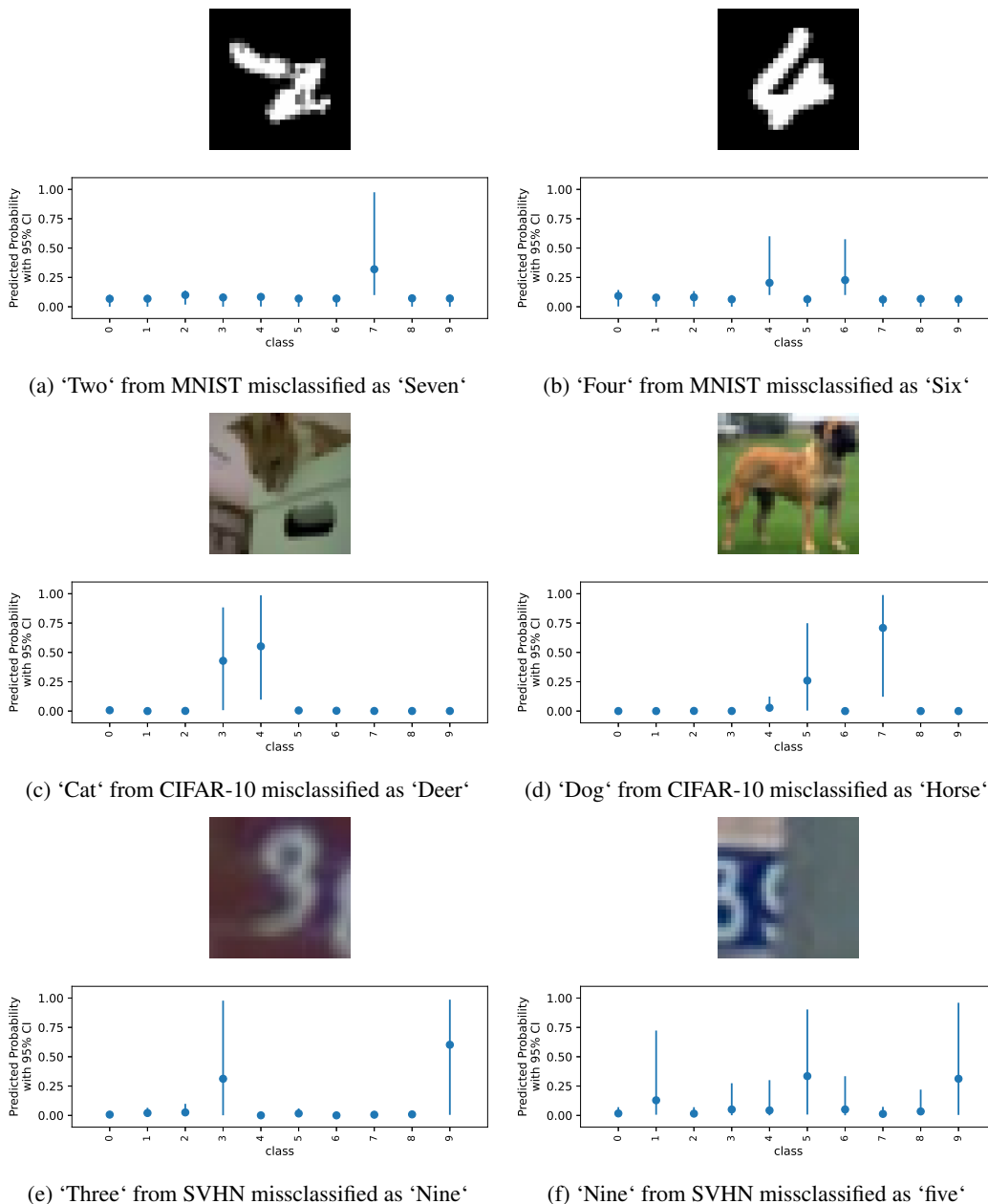


Figure 11: Examples of difficult-to-classify images from the different image data sets used. Below each image is the predictive mean for each class represented by the dot, and error bars to represent the 95% credible intervals. MNIST results fit with BPS, CIFAR-10 with σ BPS, and SVHN with Boomerang sampler using the proposed event thinning method. Best viewed on a computer screen.